Provided for non-commercial research and education use.
Not for reproduction, distribution or commercial use.

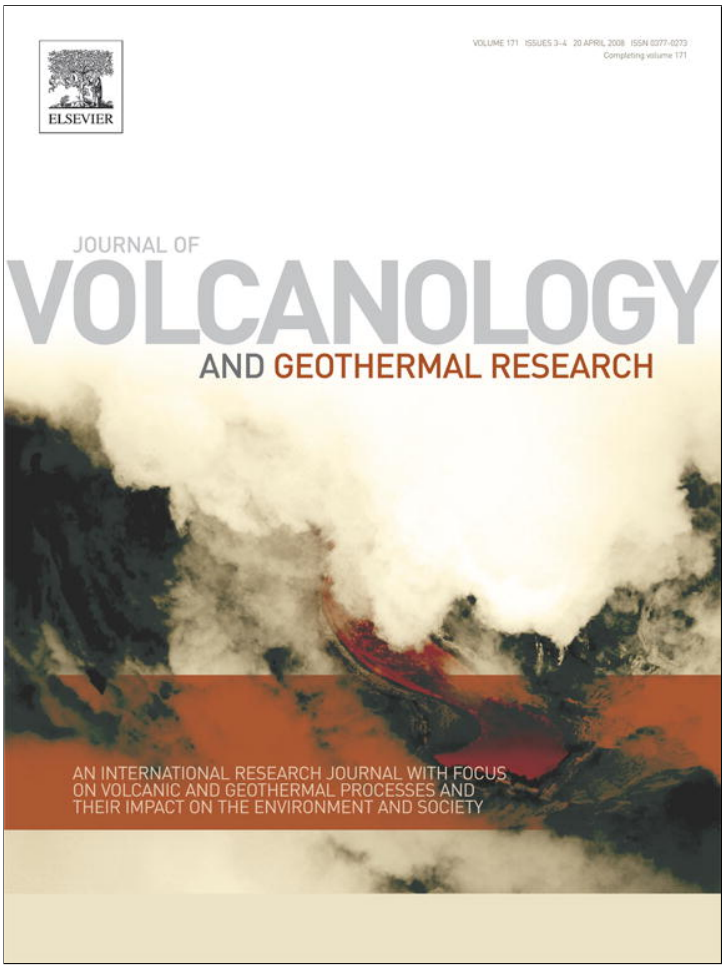


This article appeared in a journal published by Elsevier. The attached copy is furnished to the author for internal non-commercial research and education use, including for instruction at the authors institution and sharing with colleagues.

Other uses, including reproduction and distribution, or selling or licensing copies, or posting to personal, institutional or third party websites are prohibited.

In most cases authors are permitted to post their version of the article (e.g. in Word or Tex form) to their personal website or institutional repository. Authors requiring further information regarding Elsevier's archiving and manuscript policies are encouraged to visit:

http://www.elsevier.com/copyright

Author's personal copy

Available online at www.sciencedirect.com
ScienceDirect
Journal of Volcanology and Geothermal Research 171 (2008) 178–190
Journal of volcanology and geothermal research
www.elsevier.com/locate/jvolgeores

Research paper

# Six-week time series of eddy covariance $CO_2$ flux at Mammoth Mountain, California: Performance evaluation and role of meteorological forcing

J.L. Lewicki [a,*], M.L. Fischer [b], G.E. Hilley [c]

[a] Earth Sciences Division, Ernest Orlando Lawrence Berkeley National Laboratory, Berkeley, CA, 94720 USA
[b] Environmental Energy Technology Division, Ernest Orlando Lawrence Berkeley National Laboratory, Berkeley, CA, 94720 USA
[c] Department of Geological and Environmental Sciences, Stanford University, Stanford, CA, 94305 USA

Received 18 June 2007; accepted 26 November 2007
Available online 15 January 2008

**Abstract**

$CO_2$ and heat fluxes were measured over a six-week period (09/08/2006 to 10/24/2006) by the eddy covariance (EC) technique at the Horseshoe Lake tree kill (HLTK), Mammoth Mountain, CA, a site with complex terrain and high, spatially heterogeneous $CO_2$ emission rates. EC $CO_2$ fluxes ranged from 218 to 3500 g $m^{-2}$ $d^{-1}$ (mean = 1346 g $m^{-2}$ $d^{-1}$). Using footprint modeling, EC $CO_2$ fluxes were compared to $CO_2$ fluxes measured by the chamber method on a grid repeatedly over a 10-day period. Half-hour EC $CO_2$ fluxes were moderately correlated ($R^2 = 0.42$) with chamber fluxes, whereas average daily EC $CO_2$ fluxes were well correlated ($R^2 = 0.70$) with chamber measurements. Average daily EC $CO_2$ fluxes were correlated with both average daily wind speed and atmospheric pressure; relationships were similar to those observed between chamber $CO_2$ fluxes and the atmospheric parameters over a comparable time period. Energy balance closure was assessed by statistical regression of EC energy fluxes (sensible and latent heat) against available energy (net radiation, less soil heat flux). While incomplete ($R^2 = 0.77$ for 1:1 line), the degree of energy balance closure fell within the range observed in many investigations conducted in contrasting ecosystems and climates. Results indicate that despite complexities presented by the HLTK, EC can be reliably used to monitor background variations in volcanic $CO_2$ fluxes associated with meteorological forcing, and presumably changes related to deeply derived processes such as volcanic activity.
© 2007 Elsevier B.V. All rights reserved.

*Keywords:* $CO_2$ emissions; volcano monitoring; eddy covariance; chamber method; Mammoth Mountain

## 1. Introduction

The measurement of surface emissions of $CO_2$ has become an integral part of many volcanic and geothermal monitoring programs, as temporal variations in emissions may indicate changes at depth associated with volcanic activity or geothermal processes (e.g., Baubron et al., 1991; Farrar et al., 1995; Chiodini et al., 1998; Hernandez et al., 1998; Klusman et al., 2000; McGee et al., 2000; Bergfeld et al., 2001; Hernandez et al., 2001; Werner and Cardellini, 2006). Furthermore, it is important to understand the link between temporal variations in deeply derived $CO_2$ emissions, and meteorologic and hydrologic processes, as these near-surface processes can drive large changes in $CO_2$ emissions (e.g., Connor et al., 1993; McGee and Gerlach, 1998; Rogie et al., 2001; Granieri et al., 2003; Lewicki et al., 2007) that may pose health and environmental hazards or be misinterpreted to reflect changes at depth.

While the chamber method (e.g., Chiodini et al., 1998) has been reliably used to measure spatial and temporal variations in surface $CO_2$ fluxes in many volcanic and geothermal regions, limitations of the method include the measurement's small spatial scale (<1 $m^2$), alteration of the ground surface and gas flow during the measurement, and the ability to continuously monitor temporal changes in $CO_2$ fluxes at only a single or limited number of point locations within a study area. The eddy covariance (EC) method, a micrometeorological technique traditionally used to measure $CO_2$ (and other trace gas and heat) fluxes across the interface between the atmosphere and a plant canopy (e.g., Baldocchi, 2003 and references therein) has been proposed as a viable and complementary technique to

* Corresponding author. Tel.: +1 510 495 2818; fax: +1 510 486 5686.
*E-mail addresses:* jllewicki@lbl.gov (J.L. Lewicki), mlfischer@lbl.gov (M.L. Fischer), hilley@pangea.stanford.edu (G.E. Hilley).

0377-0273/$ - see front matter © 2007 Elsevier B.V. All rights reserved.
doi:10.1016/j.jvolgeores.2007.11.029

Author's personal copy



monitor volcanic $CO_2$ and heat fluxes in conjunction with the chamber method (Werner et al., 2000, 2003, 2006; Anderson and Farrar, 2001). EC provides the benefit of an automated flux measurement that does not interfere with the ground surface and is averaged over both time and space, with the spatial scale significantly larger ($m^2$–$km^2$) than that of the chamber method. Importantly, however, the theory that underlies the EC method assumes spatial homogeneity of surface fluxes, flat terrain, and temporal stationarity (e.g., Folken and Wichura, 1996), conditions that are not typically met in volcanic and geothermal environments.

Work in mountain ecosystems has shown that under suitable atmospheric conditions, EC can provide reliable $CO_2$ and heat flux measurements in complex terrain (e.g., Turnipseed et al., 2003, 2004). Werner et al. (2000, 2003) deployed EC from 1 to 2.5 weeks in the Yellowstone National Park hydrothermal system, USA and at Solfatara volcano, Italy, sites with highly heterogeneous surface $CO_2$ and heat fluxes, yet relatively flat terrain. Using footprint modeling, they showed general consistency between EC $CO_2$ fluxes and chamber $CO_2$ fluxes measured on grids, indicating that EC yielded representative measurements at these sites. However, Werner et al. (2003) suggested that the relative difference observed between the two methods could have been derived in part by incomplete characterization of the temporal variability of surface $CO_2$ fluxes within the study area by the chamber method over the EC measurement period. Anderson and Farrar (2001) performed EC measurements of $CO_2$ and heat fluxes for up to 4 days in three pilot studies at the Horseshoe Lake tree kill (HLTK) on Mammoth Mountain, USA (Fig. 1). The HLTK is a site with complex terrain and highly heterogeneous, yet cold volcanic $CO_2$ emissions, thus possessing distinctly different characteristics from the Yellowstone and Solfatara areas. While they found average EC $CO_2$ flux measurements to be generally similar to chamber measurements made in separate studies, footprint modeling as performed by Werner et al. (2000, 2003) would have been required to directly compare the results derived from these two methods.

We build on the work of Werner et al. (2000, 2003) and Anderson and Farrar (2001) by presenting a six-week time series of EC $CO_2$ fluxes measured at the HLTK. We assess the quality of EC $CO_2$ and heat flux measurements by comparing them to measurements made by independent techniques. In particular, EC $CO_2$ fluxes were compared to chamber $CO_2$ fluxes over a 10-day period when spatio-temporal variations in surface $CO_2$ fluxes were captured by repeated chamber measurements on a grid. Despite the complexities presented by the study site, we show that under certain atmospheric conditions, the EC method performs well relative to independent methods. Finally, the multi-week time series of EC fluxes allowed us to establish relationships between temporal variations in surface $CO_2$ fluxes and meteorological parameters on timescales longer than a day.

## 2. Study site

Mammoth Mountain (3368 m) is a dormant dacitic volcano formed 200,000 to 50,000 years ago on the southwestern rim of Long Valley caldera, eastern California (Fig. 1). While lavas were last erupted ~50,000 years ago, phreatic eruptions occurred up to ~700 years ago (Bailey, 1989). Recent volcanic unrest associated with Mammoth Mountain was first detected in 1979 and activity was subsequently expressed as ground deformation, swarms of small earthquakes ($M \leq 3$), spasmodic bursts, long-period and very long-period earthquakes, elevated $^3He/^4He$ ratios in fumarolic gases, and diffuse surface $CO_2$

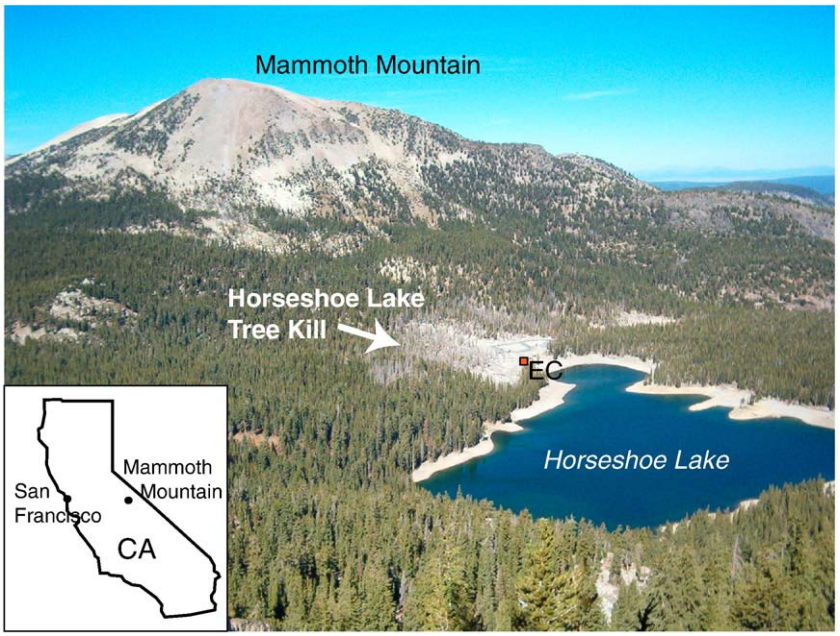


Fig. 1. View of the Horseshoe Lake tree kill located on the southeastern flank of Mammoth Mountain, adjacent to Horseshoe Lake. Red square shows approximate location of EC station.

Author's personal copy



emissions (Hill and Prejean, 2005). An eleven-month-long seismic swarm occurred at Mammoth Mountain in 1989, possibly related to dike intrusion and/or magmatic fluid migration (Hill, 1996; Hill and Prejean, 2005). Tree kills then formed in six general areas on Mammoth Mountain in 1990–1991 due to diffuse, non-thermal emissions of volcanic $CO_2$ resulting in high $CO_2$ concentrations in the root zone (e.g., Farrar et al., 1995).

The HLTK is the largest (~120,000 $m^2$) tree kill on Mammoth Mountain and is located on the northwest shore of Horseshoe Lake, on the southeast flank of the volcano (Fig. 1). It lies in the Lakes Basin, with terrain sloping upward to the west–northwest (Figs. 1 and 2). Soils here are largely barren of vegetation, 1 to 3 m thick, and composed of 0.1 to 0.4 m of pumice overlying coarse sand with cobbles to boulders and low organic carbon (McGee and Gerlach, 1998; Evans et al., 2001). Horseshoe Lake is perched, while the water table here is located at ~40 m depth (HSL-1 well; Farrar et al., 1998).

Extensive monitoring of subsurface $CO_2$ concentrations and surface $CO_2$ fluxes has been conducted at the HLTK (e.g., Farrar et al., 1995; Rahn et al., 1996; Gerlach et al., 1998; McGee and Gerlach, 1998; McGee et al., 2000; Gerlach et al., 2001; Anderson and Farrar, 2001; Rogie et al., 2001; Lewicki et al., 2007). Studies have reported large diurnal to seasonal fluctuations in time series of soil $CO_2$ concentrations, surface $CO_2$ fluxes, and total $CO_2$ discharges that appear to be due to variations in meteorological and hydrologic processes (e.g., McGee and Gerlach, 1998; McGee et al., 2000; Rogie et al., 2001). Also, Lewicki et al. (2007) showed that large spatio-temporal variations in surface $CO_2$ fluxes over multiple days can be driven by slow-moving cold fronts. Furthermore, long-term monitoring suggests that emissions have markedly declined over the past decade. For example, the average estimated $CO_2$ discharge from the tree kill area was ~250 t $d^{-1}$ for 1995 to 1997 (Gerlach et al., 1998) and 93 t $d^{-1}$ for 1997 to 2000 (Rogie et al., 2001), whereas the average discharge measured in 2006 was 38 t $d^{-1}$ (Lewicki et al., 2007).

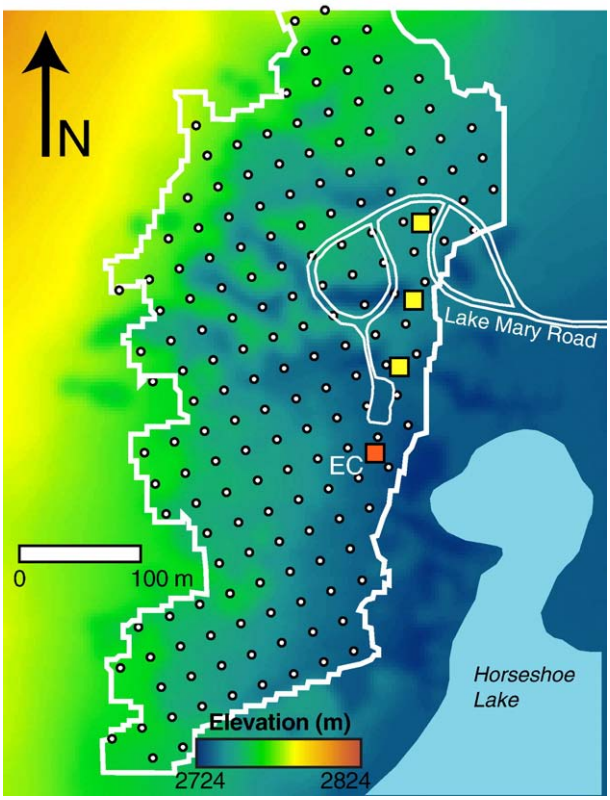


Fig. 2. Digital elevation model of the HLTK study area, outlined by white line (modified from Lewicki et al., 2007). White dots show locations of the chamber $CO_2$ flux measurement points. Red and yellow squares show approximate locations of EC stations in the present and Anderson and Farrar (2001) studies, respectively.

## 3. Methods

### 3.1. Eddy covariance measurements

An EC station (2.5 m high; see below) was deployed at the HLTK (Fig. 2) continuously from 09/08/2006 to 10/24/2006. The location of the station was chosen to take advantage of the westerly prevailing winds and the absence of asphalt road and parking lot to the west. The average surface slope to the west (from directions of 190 to 360°) and within 100 m of the station was 9% (range = 1 to 15%; Fig. 2). Within 300 m of the station, the average slope was 13% (range = 1 to 18%). Widely distributed tree stumps, rocks, and logs were located within about 50 m of the EC station. In addition, foliage-free standing dead trees, which have lost the majority of fine branches, were located from about 50 to 200 m from the EC station (Fig. 1).

The EC station was similar in design to that described by Billesbach et al. (2004) and was composed of fast-response and slow-response subsystems. The fast-response subsystem included two sensors used to measure the variables necessary to calculate turbulent fluxes of $CO_2$, $H_2O$, heat, and momentum. A Gill-Solent WindMaster Pro sonic three-dimensional anemometer/thermometer (Gill Instruments, Ltd) measured wind speeds in three directions and sonic temperature at 10 Hz. A LI-COR 7500 open-path $CO_2$–$H_2O$ infrared gas analyzer (LI-COR, Inc) measured $CO_2$ and water vapor densities at 10 Hz. Both sensors were mounted to the top of a tripod tower at 2.5 m height.

The slow-response subsystem included sensors associated with a second tripod tower that measured auxiliary variables used to compare with EC fluxes and establish relationships between EC fluxes and environmental parameters. Atmospheric pressure was measured using a Vaisala PTB101B barometer (Vaisala, Inc.). Atmospheric temperature and relative humidity were measured using a Vaisala HMP50 humidity and temperature probe. Mean horizontal wind speed and direction were measured by a Climatronics CS800-12 wind set (Climatronics Corp.) at 2.5 m height. Net radiation, total insolation and photosynthetically active radiation (PAR) were measured with a Kipp & Zonen CNR-1 radiometer (Kipp & Zonen), LI-COR LI-200SA pyranometer, and LI-COR LI-190SA quantum sensor, respectively, mounted to a horizontal bar extending from the tripod tower at 2 m height. Mean precipitation was measured by a TE525 tipping bucket rain gage (Texas Electronics). Soil moisture profiles (10 and 30 cm depth) were measured at two

Author's personal copy



locations using ECH2O (Decagon Devices) soil moisture probes. Soil temperature profiles (10, 20, and 30 cm depth) were measured at two locations with thermocouples. Soil heat flux was measured by four HFT3 soil heat flux plates (Radiation and Energy Balance Systems) located at 5 cm depth near the radiometer. Slow-response subsystem variables were measured every 5 s and averaged over 30 min for comparison with turbulent fluxes.

Carbon dioxide, latent heat (LE), sensible heat ($H$), and momentum fluxes ($F_s$) were calculated as the temporal covariance of the scalar ($s$) and vertical-wind velocity ($w$):

$$F_s = \overline{w's'} \tag{1}$$

where the overbar denotes time averaging and primes denote deviations from a mean. Fluxes were calculated for 30-minute periods. Eq. (1) gives the mean vertical turbulent flux of the scalar of interest over a horizontally homogeneous surface under steady-state conditions. Details on the theory and assumptions of the EC method can be found in Baldocchi et al. (1988), Foken and Wichura (1996), Aubinet et al. (2000) and Baldocchi (2003).

For each half-hour of data, the mean lateral ($\overline{v}$) and then the mean vertical ($\overline{w}$) wind velocities were rotated to zero (Kaimal and Finnigan, 1994). The Webb correction for the effects of fluctuation in heat and water vapor on the density of air (Webb et al., 1980) was applied. Raw signals from the infrared gas analyzer and sonic anemometer were evaluated for voltage spikes and all points more than ten standard deviations (thereby accepting a non-Gaussian tail to the data) away from a 60 s moving average were removed from the data. Turbulent fluxes measured during periods of insufficient turbulent mixing are typically underestimated. To filter data for this effect, friction velocities ($u_*$) were calculated as the square root of the momentum flux. Fig. 3 shows a plot of EC $CO_2$ flux versus $u_*$ for all EC measurements corresponding to mean wind directions from 190 to 360° (i.e., hereafter, only EC measurements corresponding to mean wind directions from the tree kill area will be considered). EC $CO_2$ fluxes increase sharply with $u_*$ until $u_* \sim 0.25$ m s$^{-1}$, above which EC fluxes remain relatively constant (Fig. 3). We eliminated all EC ($CO_2$ and heat) fluxes corresponding to $u_* \leq 0.25$ m s$^{-1}$. A test for stationarity was conducted according to Foken and Wichura (1995). Each 30-minute EC flux measurement was divided into six 5-minute segments. If the difference between the average of the six 5-minute segments and the 30-minute measurement was greater than 30%, the measurement was considered non-stationary and discarded. Specific details of data filtering are also shown on each of the following figures.

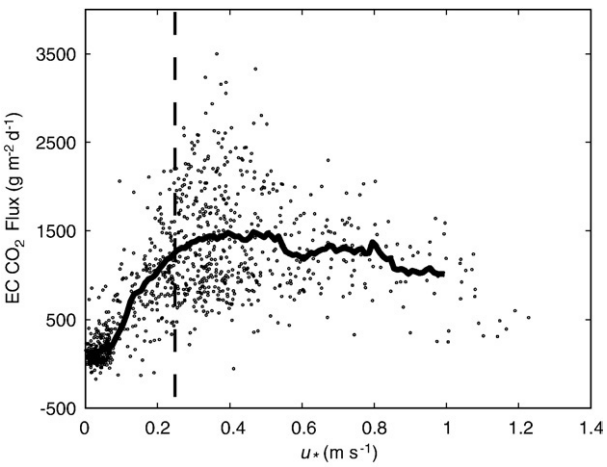


Fig. 3. Plot of EC $CO_2$ flux versus friction velocity ($u_*$). Solid line is running average of EC $CO_2$ flux over a 0.1 m s$^{-1}$ $u_*$ window. Vertical dashed line shows $u_*$=0.25 m s$^{-1}$.

### 3.2. Chamber measurements

Surface $CO_2$ flux was measured using a WEST Systems fluxmeter (WEST Systems) based on the chamber method, with repeatability of ±10% (Chiodini et al., 1998). Evans et al. (2001) conducted laboratory measurements of imposed $CO_2$ fluxes over a range typical of Mammoth Mountain tree kill areas through a synthetic "soil" similar in properties to surficial deposits in the tree kill areas, and showed that chamber measurements were negatively biased, on average by 12.5%. Collars were not used for chamber measurements, due to the potential alteration of soil properties and gas flow (e.g., Gerlach et al., 2001). Surface $CO_2$ flux was measured at 170 grid points at 27-m spacing in the HLTK (Fig. 2). Flux measurements were repeated in the same order along the grid each day from 09/12/2006 to 09/21/2006 between 07:00 and 15:00, with the exception of 09/15/2006 when no measurements were made. For the purpose of comparison with EC $CO_2$ fluxes, the negative bias in chamber measurements was corrected for by increasing each flux measurement by 12.5%. A map of surface $CO_2$ flux was then produced for each day of grid measurements using nearest neighbor interpolation at 5×5 m resolution, chosen for its simplicity in the comparison of chamber to EC $CO_2$ flux measurements. Surface $CO_2$ flux maps produced using the sequential Gaussian simulation method and corresponding total $CO_2$ discharges from the study area are presented in Lewicki et al. (2007). For reference, Lewicki et al. (2005) presented a comparison of a range of geostatistical interpolation and simulation methods that were applied to chamber $CO_2$ fluxes measured in a volcanic environment.

## 4. Results

### 4.1. Meteorology

Atmospheric temperatures ranged from −8.3 to 20.8 °C and winds were dominantly from the west (Fig. 4) over the study period. The highest wind speeds were measured from westerly directions, while easterly winds typically corresponded to relatively low wind speeds (Fig. 4). Precipitation (typically light snow) occurred on 6 days during October (10/01/2006, 10/02/2006, 10/10/2006, 10/11/2006, 10/14/2006, and 10/17/2006) (Figs. 5b and 7). Average daily wind speeds and atmospheric pressures varied from 1.1 to 3.5 m s$^{-1}$ and 725 to 740 mbar, respectively from 09/08/2006 to 10/24/2006 (Fig. 5a). A cold front

Author's personal copy



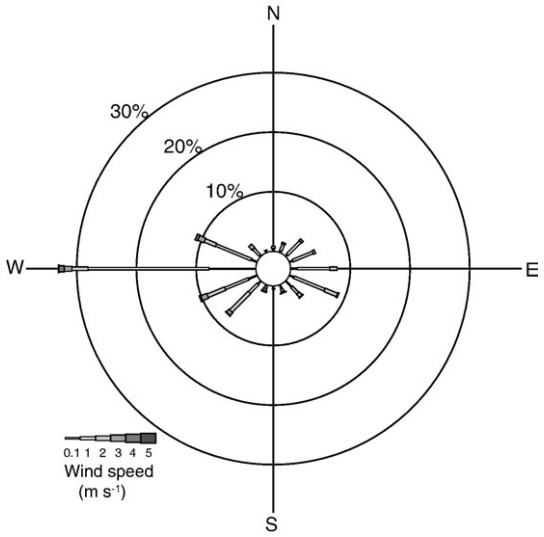


Fig. 4. Wind rose showing joint frequency distribution of mean horizontal wind speed and direction (half-hour averages) from 09/08/2006 to 10/24/2006, constructed using Frequency Works.

occurred on 09/14/2006 to 09/15/2006 (Lewicki et al., 2007) and was accompanied by high average daily wind speeds and low atmospheric pressures (see zone I on Fig. 5a). Over the entire measurement period (09/08/2006 to 10/24/2006), average daily wind speeds and atmospheric pressures were moderately inversely correlated (correlation coefficient = −0.43). From 09/08/2006 to 09/22/2006 (zone I, Fig. 5a), average daily wind speed and pressure were strongly inversely correlated (correlation coefficient = −0.80). Relationships between meteorological parameters and chamber $CO_2$ fluxes over this time period were examined in Lewicki et al. (2007). We therefore selected this time frame to analyze relationships between meteorological parameters and EC $CO_2$ fluxes for comparison. From 09/24/2006 to 10/10/2006 (zone II, Fig. 5a), average daily wind speed and pressure were poorly correlated (correlation coefficient = 0.14). We selected zone II to examine correlations between average daily wind speed, pressure, and EC $CO_2$ fluxes because of different meteorological conditions (i.e., lack of a cold front) from zone I, and a sufficient number of EC data to perform the analysis.

### 4.2. Chamber fluxes

Large spatio-temporal variations in surface $CO_2$ fluxes were measured using the chamber method from 09/12/2006 to 09/21/2006 (Figs. 5b and 6). During the first 2 days of measurements (09/12/2006 and 09/13/2006), the spatial distribution of surface $CO_2$ fluxes remained relatively stable (Fig. 6ab). Then, on 09/14/2006 surface $CO_2$ fluxes decreased and the region of relatively high flux began to contract in size (Figs. 5b and 6c). On 09/16/2006, surface $CO_2$ fluxes continued to decrease and the region of elevated flux further contracted in size (Figs. 5b and 6d). $CO_2$ fluxes then increased and the region of elevated $CO_2$ flux expanded outwards on 09/17/2006 to 09/18/2006 (Figs. 5b and 6e–f). With the exception of 09/19/2006, surface $CO_2$ fluxes continued to increase over the remainder of the measurement period (Figs. 5b and 6g–i). Further details on the spatio-temporal variations in chamber $CO_2$ fluxes are found in Lewicki et al. (2007).

### 4.3. Eddy covariance $CO_2$ fluxes

EC $CO_2$ fluxes measured from 09/08/2006 to 10/24/2006 ranged from 218 to 3500 g m$^{-2}$ d$^{-1}$ (Fig. 7), with a mean and standard deviation of 1346 and 575 g m$^{-2}$ d$^{-1}$, respectively. Large gaps in the time series of $CO_2$ fluxes were present due to

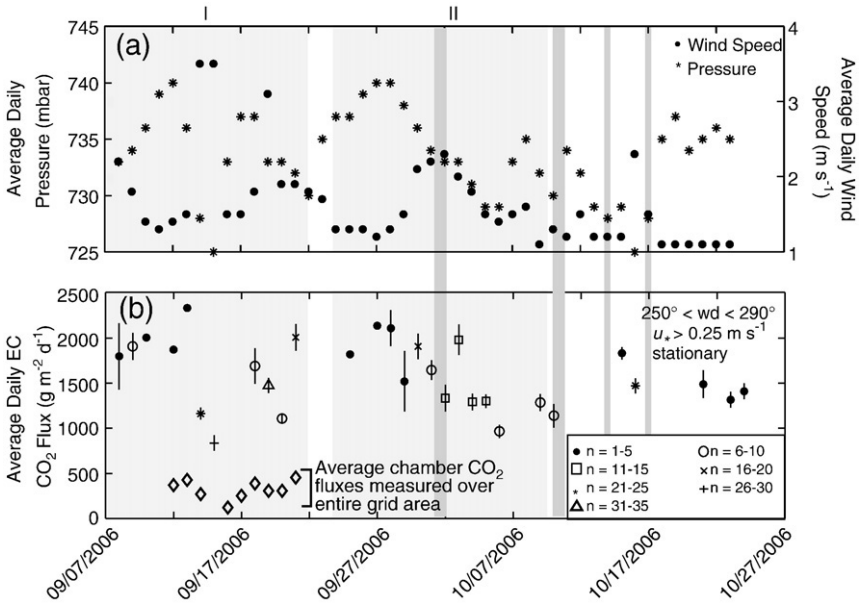


Fig. 5. (a) Time series of average daily atmospheric pressure (stars) and wind speed (dots). (b) Time series of average daily EC $CO_2$ flux corresponding to wind directions from 250 to 290°. Symbols indicate number of measurements ($n$) used to calculate average daily EC $CO_2$ fluxes. Error bars are standard error of mean. Average daily EC $CO_2$ fluxes are missing on days where filtering has entirely eliminated half-hour data. Diamonds are average of chamber $CO_2$ fluxes measured repeatedly on daily basis over entire grid area grid from 09/12/2006 to 09/21/2006. Dark gray zones indicate approximate timing of precipitation events. See text for explanations of light grayed zones I and II.

Author's personal copy



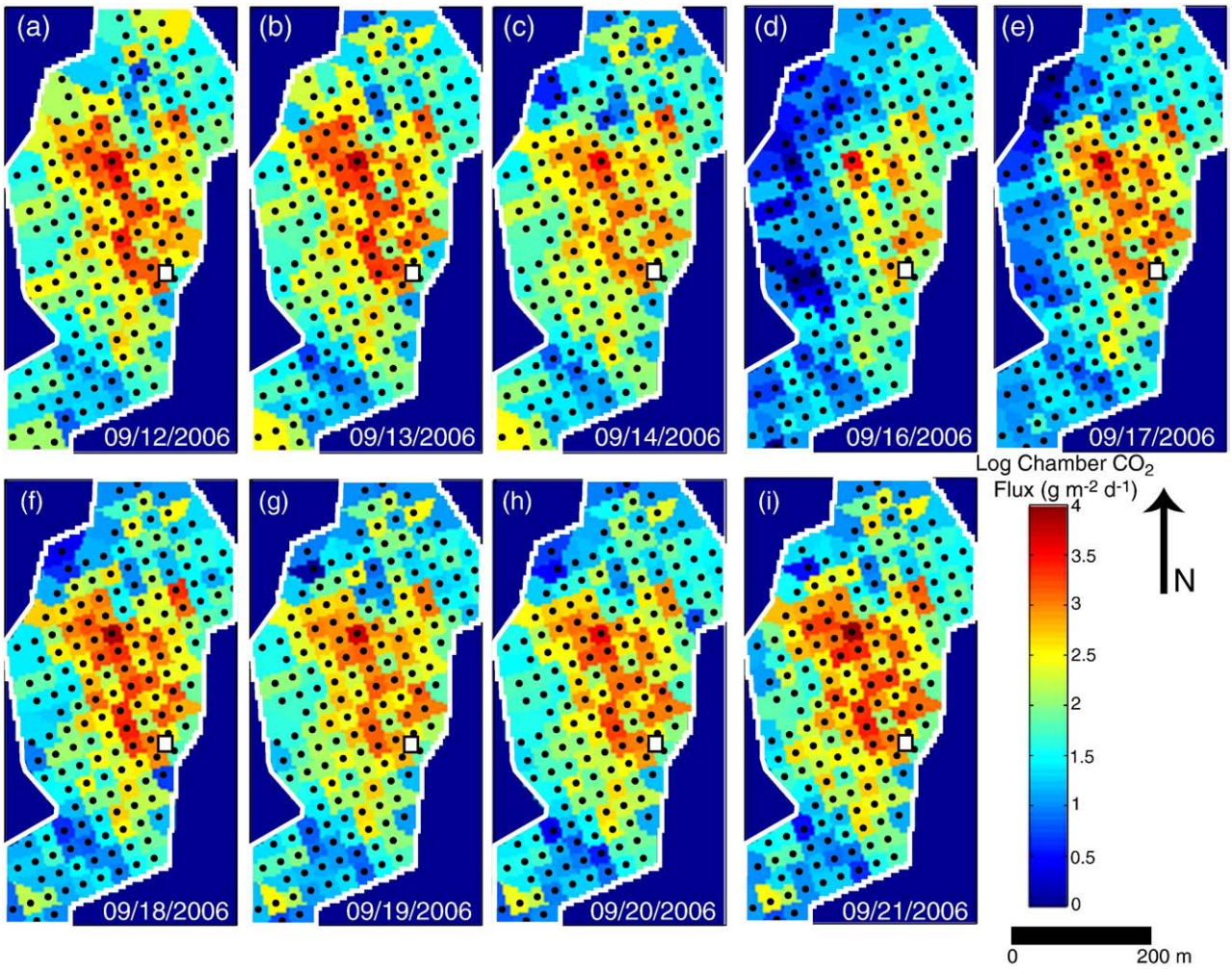


Fig. 6. (a–i). Time series (09/12/2006 to 09/21/2006) of maps of log chamber $CO_2$ flux. White squares denote approximate location of EC station.

filtering for mean horizontal wind direction, $u_*$, and stationarity. For example, 47% of the EC $CO_2$ fluxes corresponding to wind directions from 190 to 360° were lost due to filtering for $u_*$ and stationarity.

### 4.4. Comparison of eddy covariance to chamber $CO_2$ fluxes

The vertical scalar flux (e.g., of $CO_2$; $F_{CO_2}$) measured by EC at point ($x_m$, $y_m$, $z_m$) is the integral of the contributions from all upwind surface $CO_2$ emissions. The relative weight of each surface point source emission on $F_{CO_2}$ depends on its location relative to the EC instrumentation. $F_{CO_2}$ is related to the distribution of source $CO_2$ fluxes at the surface ($x'$, $y'$, $z'=z_0$) with strength $Q_{CO_2}$ by the footprint function or source weight function, $f(x_m-x', y_m-y', z_m-z_0)$:

$$F_{CO_2}(x_m, y_m, z_m) = \int_{-\infty}^{\infty}\int_{-\infty}^{\infty} Q_{CO_2}(x', y', z'=z_0) \cdot f(x_m - x', y_m - y', z_m - z_0) \cdot dx' \cdot dy' \quad (2)$$

(e.g., Horst and Weil, 1992; Schmid, 1997). The value of the footprint function generally rises to a maximum some distance upwind of the EC sensors, then smoothly falls off in all directions. The total surface influence on $F_{CO_2}$, or the source area, is the integral beneath the footprint function.

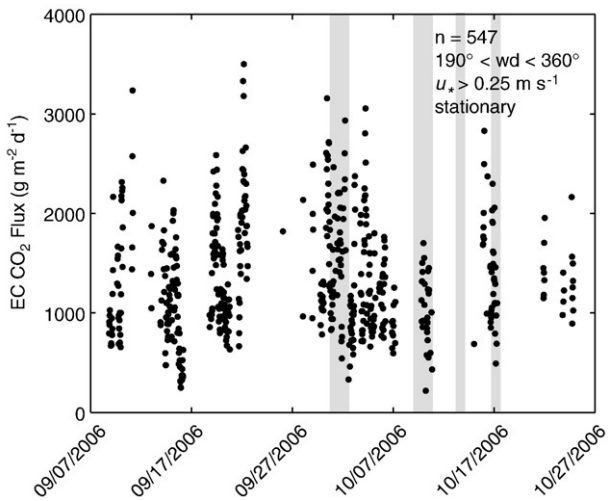


Fig. 7. Time series of EC $CO_2$ flux corresponding to mean wind direction between 190 and 360°, $u_*>0.25$ m s$^{-1}$, and stationary measurements. Gray zones indicate approximate timing of precipitation events.

Author's personal copy



Table 1
Daily averages of half-hour data used for EC-footprint $CO_2$ flux comparisons and mean vertical-wind speed

| Date | $n$ | EC $CO_2$ flux ($g\ m^{-2}\ d^{-1}$) | Footprint $CO_2$ flux ($g\ m^{-2}\ d^{-1}$) | $L$ (m) | $u_*$ ($m\ s^{-1}$) | $\sigma_v$ ($m\ s^{-1}$) | Wind direction (°) | $\overline{w}$ ($m\ s^{-1}$) |
|---|---|---|---|---|---|---|---|---|
| 09/12/2006 | 3 | 1437.3 | 1327.9 | −63.7 | 0.32 | 1.4 | 263 | −0.05 |
| 09/13/2006 | 5 | 1252.2 | 1134.5 | −62.5 | 0.32 | 1.4 | 225 | $0.03e^{-1}$ |
| 09/14/2006 | 23 | 856.8 | 1006.0 | −1415.3 | 0.88 | 3.0 | 263 | −0.26 |
| 09/18/2006 | 7 | 1032.4 | 1163.1 | −76.9 | 0.37 | 1.5 | 236 | −0.06 |
| 09/19/2006 | 14 | 1059.3 | 1061.4 | −491.2 | 0.82 | 2.7 | 265 | −0.25 |
| 09/20/2006 | 7 | 964.1 | 1060.5 | −40.2 | 0.32 | 1.6 | 268 | −0.09 |
| 09/21/2006 | 14 | 1436.4 | 1425.2 | −60.4 | 0.51 | 1.9 | 262 | −0.13 |

Similar to the methods of Werner et al. (2000, 2003), we compared EC with chamber measurements of $CO_2$ flux by modeling the footprint function for each half-hour EC measurement from 09/12/2006 to 09/21/2006. The Flux Source Area Model (FSAM) of Schmid (1997), based on analytic solutions of the advection–diffusion equation (Horst and Weil, 1992) was used to model footprint functions using the following inputs: (1) $z_m = 2.5$ m; (2) surface roughness height, $z_0 = 0.03$ m, in accordance with Anderson and Farrar (2001); (3) measured mean horizontal wind direction; (4) cross-wind turbulence near the surface characterized by calculated $\sigma_v/u_*$, where $\sigma_v$ is the standard deviation of the wind speed in the cross-wind direction; (5) calculated Monin–Obukhov length, $L$, if corresponded to unstable atmospheric conditions (i.e., only measurements corresponding to $L<0$ were considered) (Table 1). We calculated $f$ at the center of each 25-$m^2$ grid block in Fig. 6. The source area was defined here as the area within which 90% of the measured EC flux was derived from. Results indicated that the source area was located within ~100 m upwind of the EC station for all of the 73 footprint functions modeled (mean = 86 m, range = 26 to 108 m; Fig. 8). In other words, the source area was contained within the tree kill area for all modeled footprint functions.

On each day from 09/12/2006 to 09/21/2006, $Q_{CO_2}$ was assumed equal to the chamber $CO_2$ flux in Fig. 6. The product of $Q_{CO_2}$ and $f$ was then calculated for each 25-$m^2$ grid block and summed over the source area, yielding the "footprint $CO_2$ flux". Fig. 9 shows a histogram of the relative difference between the measured EC $CO_2$ flux and the footprint $CO_2$ flux, expressed as a percent of the EC flux. The mean relative difference was −0.3%, with a standard error = 2.7%. The standard deviation of the relative difference was 23% and the mode was offset positively from zero. No systematic relationship was observed between the relative difference and $L$, $u_*$, time of day, or wind direction for the ranges of values considered. A plot of EC versus footprint $CO_2$ flux (Fig. 10a) shows that the data were moderately correlated ($R^2 = 0.42$ for 1:1 line). At $CO_2$ flux up to ~1300 $g\ m^{-2}\ d^{-1}$, the data clustered around the 1:1 line, while at higher flux, EC $CO_2$ fluxes tended to be biased high relative to footprint $CO_2$ fluxes. Mean vertical-wind velocities ($\overline{w}$) corresponding to the modeled footprints ranged from −0.43 to 0.03 $m\ s^{-1}$ (mean and standard deviation = −0.17 and 0.12 $m\ s^{-1}$, respectively). $\overline{w}$ was negatively correlated (correlation coefficient = −0.37) with the relative difference between the EC and footprint $CO_2$ fluxes, such that EC $CO_2$ fluxes were typically greater than footprint fluxes when $\overline{w}$ was more negative.

The correlation of average daily EC and average daily footprint $CO_2$ flux increased substantially ($R^2 = 0.70$ for 1:1 line) relative to half-hour measurements, while the positive bias at flux >1300 $g\ m^{-2}\ d^{-1}$ was reduced (Fig. 10b). Furthermore, the correlation between average daily $\overline{w}$ (Table 1) and the relative difference between EC and footprint $CO_2$ fluxes was reduced (correlation coefficient = 0.24) relative to half-hour measurements.

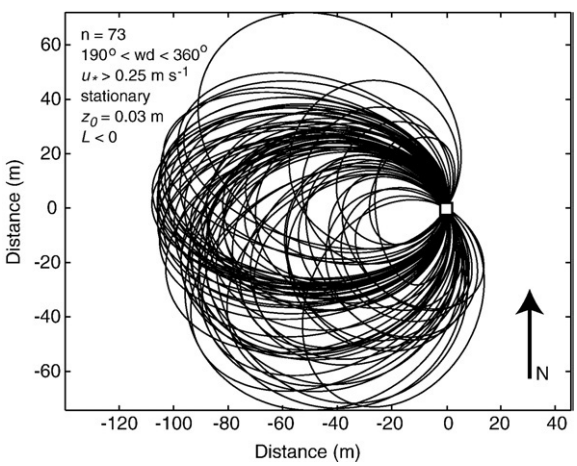


Fig. 8. Source areas (area within which 90% of the measured EC flux was derived from) for 73 modeled footprints. Square shows location of EC station.

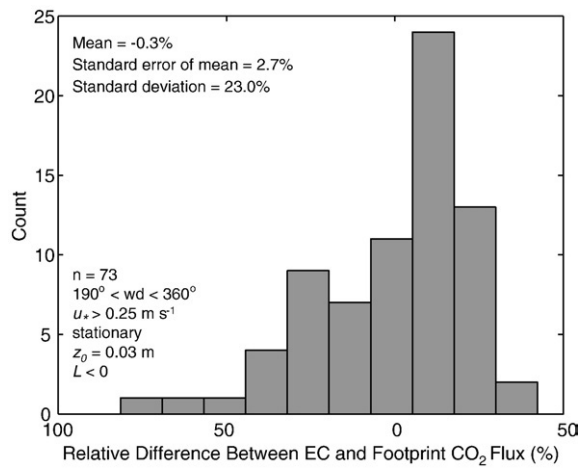


Fig. 9. Histogram of the relative difference between EC and footprint $CO_2$ fluxes, expressed as percent of EC flux.

Author's personal copy



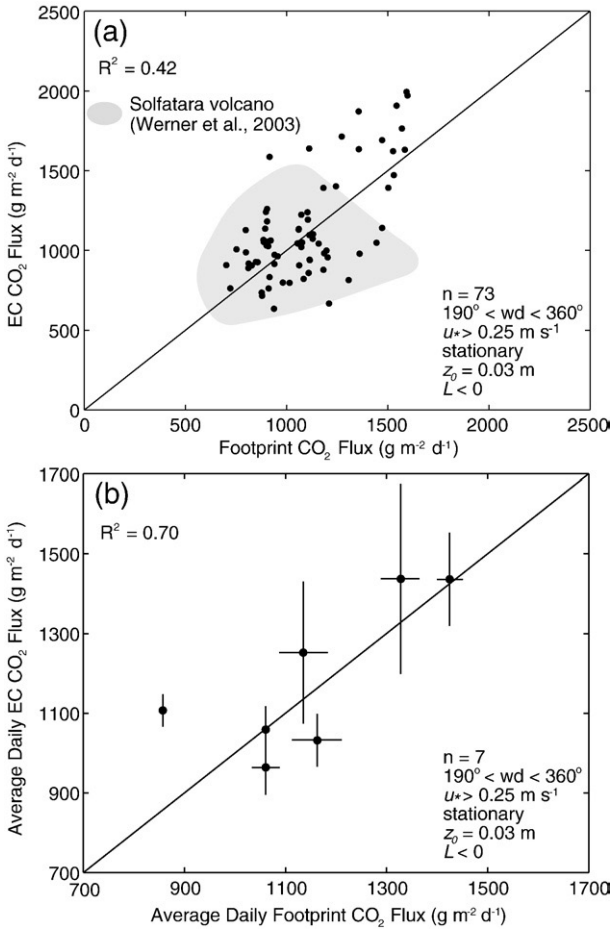


Fig. 10. Plots of (a) EC $CO_2$ flux versus footprint $CO_2$ flux for half-hour EC measurements and (b) average daily EC $CO_2$ flux versus average daily footprint $CO_2$ flux. Error bars show standard error of mean. Gray area encompasses data from diffusely degassing areas at Solfatara volcano, Italy (Location 1; Werner et al., 2003).

### 4.5. Relationships between temporal variations in EC $CO_2$ fluxes and meteorology

To assess the relationships between temporal variations in meteorological parameters and EC $CO_2$ fluxes, we calculated average daily EC $CO_2$ fluxes from 09/08/2006 to 10/24/2006 using fluxes corresponding to a narrow range of mean horizontal wind directions (250 to 290°; Fig. 5b). Since the source area changes for each EC flux measurement depending on atmospheric conditions, a time series of EC fluxes is influenced by both temporal variations in, and spatial heterogeneity of, surface fluxes. This spatial component can complicate comparison of temporal variations in EC $CO_2$ fluxes to meteorological (or deep volcanic, hydrothermal) processes. Therefore, to limit the effects of spatial heterogeneity of surface fluxes on the evaluation of temporal variability of EC $CO_2$ fluxes, we only considered fluxes corresponding to a narrow range of mean horizontal wind directions (250 to 290°) in the calculation of average daily EC $CO_2$ fluxes (Fig. 5b). However, in this simple analysis, it was not possible to assess changes in the same flux source area over time.

No systematic relationship was observed between average daily EC $CO_2$ flux and average daily atmospheric or soil temperature. A decrease in average daily and half-hour EC $CO_2$ fluxes was observed during precipitation events on 10/01/2007–10/02/2007 and 10/10/2007–10/11/2007 and in half-hour measurements on 10/17/2007 (Figs. 5b and 7). Changes in EC flux associated with snowfall on 10/14/2007 were not possible to assess due to gaps in the time series of EC flux. From 09/08/2006 to 10/24/2006, average daily EC $CO_2$ flux was most strongly positively correlated with average daily atmospheric pressure (correlation coefficient = 0.52) and inversely correlated with average daily wind speed (correlation coefficient = −0.33) at 1-day time lag (Fig. 5a and b). From 09/08/2006 to 09/22/2006 (zone I, Fig. 5a and b), average daily EC $CO_2$ flux was more strongly correlated with average daily wind speed (correlation coefficient = −0.70) than with average daily atmospheric pressure (correlation coefficient = 0.57). However, from 09/24/2006 to 10/10/2006 (zone II, Fig. 5a and b), EC $CO_2$ flux was more strongly correlated with atmospheric pressure (correlation coefficient = 0.64) than with wind speed (correlation coefficient = −0.39).

### 4.6. Eddy covariance heat fluxes

Measured $H$ from 09/08/2006 to 10/24/2006 ranged from −91.9 to 466 W $m^{-2}$, with a mean and standard deviation of 52.2 and 106.2 W $m^{-2}$, respectively. Measured $LE$ ranged from −99.9 to 176.4 W $m^{-2}$, with a mean and standard deviation of 19.3 and 34.7 W $m^{-2}$, respectively.

Neglecting the heat stored in the air beneath the sensors and horizontal advection, the one-dimensional energy balance for the tree kill can be written as:

$$Rn - G = LE + H, \tag{3}$$

where $Rn$ and $G$ are the net radiation and heat flux into the soil, respectively. Their difference represents the available energy. Fig. 11 shows $LE+H$ versus $Rn-G$ measured at the HLTK from 09/08/2006 to 10/24/2006. Data were categorized based on time of day using PAR measurements and atmospheric stability using the stability parameter $\xi$

$$\xi = \frac{z_m - d}{L} \tag{4}$$

(Garratt, 1992). $d$ is the zero-plane displacement, estimated as 63% of canopy height, which we assumed to equal zero based on absence of a canopy within the much of the source areas. Measured turbulent heat fluxes were well correlated with available energy ($R^2$ = 0.77 for 1:1 line). We calculated the relative difference between $H$+LE and Rn−$G$, expressed as percent of $H$+LE. Systematic energy imbalances were observed, depending on time of day and atmospheric stability. The mean relative difference for energy fluxes measured at night was 44.1%. For fluxes measured during the day during neutral and stable conditions ($\xi > -0.1$), the mean relative difference was −47.3%, whereas it was −34.8% for fluxes measured during unstable-daytime ($\xi \leq -0.1$) periods. No systematic

Author's personal copy



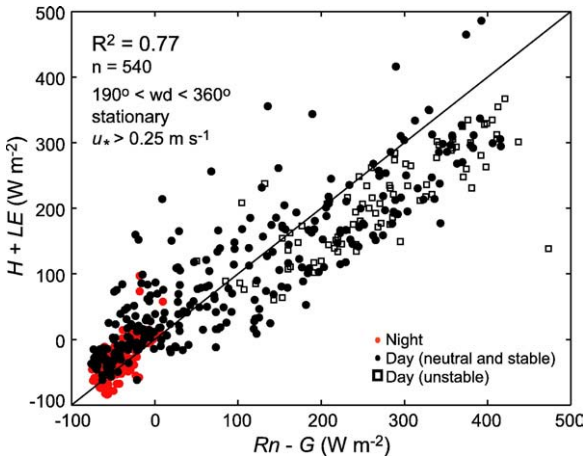


Fig. 11. Plot of sum of latent (*LE*) and sensible (*H*) heat flux measured by EC versus difference between net radiation (Rn) and soil heat flux (*G*) measured by radiometer and heat flux plates, respectively from 09/12/2006 to 09/21/2006. Red dots are measurements made during the nighttime. Black dots and squares are measurements made during neutral-and-stable-daytime ($\xi > -0.1$) and unstable-daytime ($\xi \leq -0.1$) periods, respectively. 1:1 line is shown.

relationships were observed between $\overline{w}$ and the relative difference between $H+$LE and Rn$-G$.

## 5. Discussion

### 5.1. Performance evaluation of eddy covariance

The average $CO_2$ flux (1346 g m$^{-2}$ d$^{-1}$) measured by EC from 09/08/2006 to 10/24/2006 at the HLTK (Fig. 7) fell within the range of average fluxes (691 to 1382 g m$^{-2}$ d$^{-1}$) measured by Anderson and Farrar (2001) during their three sampling campaigns in 1996–1998. While the general similarity of measured values is encouraging, direct comparison of the two studies is not possible due to the different flux source areas that were sampled in the two studies. For example, the EC stations in the Anderson and Farrar (2001) study were located north of our EC station (Fig. 2); thus, portions of asphalt parking lot were likely located within their flux source areas. In addition, comparison of EC fluxes measured in the different studies will also be complicated by the large spatial–temporal variations in surface $CO_2$ fluxes that occur within the tree kill on diurnal to inter-annual timescales (e.g., Gerlach et al., 1998; Rogie et al., 2001; Lewicki et al., 2007).

We used footprint modeling to compare EC to chamber measurements of $CO_2$ fluxes at the HLTK. With a mean relative difference of $-0.3\pm2.7\%$ between half-hour EC and footprint $CO_2$ fluxes (Fig. 9), the measurements were on average nearly unbiased. At relatively high flux, half-hour EC $CO_2$ fluxes tended to be biased high, relative to footprint $CO_2$ fluxes. Also, datasets for the HLTK were moderately correlated (Fig. 10a), with a variance in the relative difference of 23%. Table 2 shows relative differences between EC and chamber $CO_2$ fluxes in volcanic and hydrothermal systems. Using footprint models to compare chamber to EC $CO_2$ fluxes, the Werner et al. (2000, 2003) investigations are most analogous to this study. Our results for the HLTK were similar to those reported by Werner et al. (2003) for diffusely degassing areas of Solfatara volcano, Italy (Fig. 10a; Table 2). On average, a larger relative difference was observed between EC and chamber $CO_2$ fluxes for the Yellowstone National Park data, likely due in part to the presence of hydrothermal features within the EC source areas (Werner et al., 2000). Also, a larger dataset would be required for Yellowstone for closer comparison with other studies. While Anderson and Farrar (2001) did not directly compare EC to chamber $CO_2$ fluxes at the HLTK based on footprint modeling, they reported relative differences between average EC $CO_2$ fluxes calculated for the duration of their pilot studies and average chamber $CO_2$ fluxes measured in independent studies. Based on this analysis, they reported significantly larger negative bias in EC relative to chamber flux measurements than reported in other studies (Table 2).

Several factors may account for the differences observed between half-hour EC and footprint $CO_2$ fluxes (Figs. 9 and 10a). First, both the EC method and the analytic footprint model assume homogeneous surface fluxes, flat terrain, and uniform surface roughness. However, systematic errors associated with violations to these assumptions could be difficult to diagnose because they will depend on interactions between terrain, wind direction and speed, and atmospheric stability. EC fluxes were on average unbiased relative to footprint fluxes and no systematic relationship was observed when comparing the relative difference between the EC and footprint $CO_2$ fluxes and the ranges of $L$, $u_*$, time of day, or wind direction considered in the analysis. However, we observed positive bias of EC relative to footprint $CO_2$ fluxes at relatively high flux. Also, the relative difference between EC and footprint $CO_2$ fluxes increased as $\overline{w}$ became more negative. Non-zero $\overline{w}$ values can be indicative of

Table 2
Relative differences for EC and chamber $CO_2$ flux comparisons in volcanic and hydrothermal systems

| Site | Mean ± standard deviation relative difference between EC and chamber $CO_2$ fluxes | *n* | Reference |
|---|---|---|---|
| Yellowstone National Park, USA | −4.1±68% | 6 | Werner et al. (2000) |
| Solfatara volcano, Italy | −0.4±32% | 66 | Werner et al. (2003) |
| Mammoth Mountain, USA | −19 to −40% | 2 | Anderson and Farrar (2001) |
| Mammoth Mountain, USA | −0.3±23% | 73 | Present study |

For Werner et al. (2000, 2003) and the present study, the relative difference is defined as the half-hour EC $CO_2$ flux minus footprint $CO_2$ flux, expressed as percent EC $CO_2$ flux. The mean and standard deviation of these values are reported. For Anderson and Farrar (2001), the relative difference is the mean EC $CO_2$ flux for study duration (two pilot studies were considered) minus the mean chamber $CO_2$ flux measured in independent studies, expressed as percent mean EC $CO_2$ flux. Only the range of these values is reported.

Author's personal copy



advective flux (e.g., Lee, 1998; Turnipseed et al., 2003), but interpretations of their effect on EC fluxes vary. Lee (1998) suggested that horizontal flow divergence below the EC measurement height caused negative $\overline{w}$ and loss of $CO_2$ flux at night under stable conditions over a deciduous forest. However, over a coniferous forest in mountainous terrain, Turnipseed et al. (2003) interpreted positive $\overline{w}$ values and loss of $CO_2$ flux at night under stable stratification to reflect flow convergence near the EC tower due to local changes in terrain. We only deployed a single EC station, and so we cannot assess the horizontal advective fluxes necessary to close the conservation of mass equations that would be required to understand the sign and cause of the bias we observe. We suspect that the negative bias in $\overline{w}$ and positive bias in EC $CO_2$ flux at high flux we observe under unstable conditions likely result from air flow changes as wind interacts with the complicated terrain of the study area. Presumably, a planar-fit coordinate rotation (Wilczak et al., 2001) could be used to reduce vertical-wind bias. Finally, the effects of wind drag on downhill horizontal flows would likely only subtly affect wind speed gradients, since standing dead wood within the EC source areas was sparsely distributed and free of foliage and fine branches. In fact, the observed negative bias in $\overline{w}$ is opposite to what we might expect if wind drag slowed airflow and forced up-flow near the EC station.

Second, aspects of the chamber method can lead to underestimation or overestimation of soil $CO_2$ fluxes. For example, fluxes measured by vented chambers can be systematically high during windy times due to Venturi effects (e.g., Conen and Smith, 1998). While we cannot rule this effect out for all measurements, we did not find evidence for systematic overestimation of chamber $CO_2$ fluxes at the HLTK. In addition, some infiltration of atmospheric air into the chamber during windy periods could have occurred, biasing chamber $CO_2$ fluxes low. However, this effect would not account for the spatially systematic decrease in soil $CO_2$ flux that was observed on 09/14/2007 with high average daily wind speed, and then following the passage of the cold front on 09/16/2007 when low average daily wind speed was observed (Fig. 6, Lewicki et al., 2007). Rather, we would expect wind-driven air infiltration into the chamber to affect chamber flux measurements randomly over the study area. Placement of the chamber on the soil surface disturbs the soil properties and gas flow during the time of measurement, which can lead to systematically low flux measurements when advective soil gas flow occurs (Welles et al., 2000; Evans et al., 2001). While we attempted to correct chamber measurements for this effect prior to the footprint analysis, it is possible that chamber fluxes were under-corrected at relatively high flux, thus potentially contributing to the high EC relative to footprint $CO_2$ fluxes.

Third, we demonstrated that large variations occur in the spatial distribution and magnitude of surface $CO_2$ fluxes over relatively short periods of time within the tree kill area (Fig. 6), which are difficult to characterize with the chamber method, even when measurements are repeated on a daily basis. As a result, our assumption that on any given day, over the entire day, the distribution of source $CO_2$ fluxes is equal to the measured chamber fluxes on that day probably introduced error into the comparison. Finally, random errors associated with both the EC and chamber methods (e.g., Chiodini et al., 1998; Baldocchi, 2003) were likely important sources of variability in the comparison. Nonetheless, given all of the complexities of the HLTK site, it is encouraging that relatively small biases exist in our dataset, which reinforces our assertion that the EC method may be used with some success in such environments.

When the half-hour EC and footprint $CO_2$ fluxes were averaged over daily timescales, the correlation improved substantially (Fig. 10b). Also, the positive bias observed at relatively high flux in half-hour EC relative to footprint $CO_2$ fluxes was reduced in the average daily fluxes. Since each grid of chamber measurements was typically completed over ~8 h on a given day, averaging EC and footprint $CO_2$ fluxes over day-long periods allowed us to evaluate the measurements over more comparable timescales. This likely contributed to the improved correlation observed between average daily EC and footprint $CO_2$ fluxes. Our results suggest that if monitoring variations in surface $CO_2$ fluxes over timescales longer than a day is adequate for the investigation of interest (e.g., volcano monitoring), then the EC technique can perform well under certain complex site conditions.

Average $H$ and $LE$ values measured from 09/08/2006 to 10/24/2006 fell within the range of average values measured by Anderson and Farrar (2001) during their three sampling campaigns at the HLTK. These values were lower than those measured by Werner et al. (2006) at Solfatara volcano, which is expected due to the relatively high soil temperatures and steam condensation in soils in the Solfatara hydrothermal area. Also, Werner et al. (2006) found that measurements of $H$ and $LE$ were positively correlated with EC $CO_2$ fluxes in the Solfatara hydrothermal area, reflecting a large volcanic component in all fluxes. We found no systematic relationship between these parameters at the HLTK, due to the different sources of heat (non-volcanic) and $CO_2$ (volcanic).

We further assessed the performance of EC at the HLTK by comparing EC heat flux measurements to measurements made by independent methods. While the degree of energy balance closure obtained in the field is directly applicable to evaluation of $H$ and $LE$, its utility in the evaluation of $CO_2$ fluxes will depend on whether sources of error are associated with the EC method or in determining the available energy terms (e.g., Wilson et al., 2002). The degree of energy balance closure observed (Fig. 11) fell within the range of that observed at FLUXNET sites, where energy fluxes were measured over a wide range of ecosystems and climates, typically with more ideal terrain and surface flux characteristics than observed at the HLTK (Wilson et al., 2002). Turbulent heat fluxes at the tree kill were typically underestimated relative to available energy during daytime hours, whereas during nighttime hours, turbulent heat fluxes were overestimated relative to available energy.

Lack of complete energy balance closure can result from a range of issues, including systematic and random sampling errors, lack of complete estimation of heat stored beneath the EC sensors, inherent low and high pass filtering associated with

Author's personal copy



the EC method, and advection of heat induced by horizontal heterogeneity of surface fluxes and complex terrain (e.g., Wilson et al., 2002). While it is not possible to unequivocally determine the sources of error and their relative importance in the energy balance assessment, one or more issues could be relevant to the HLTK area. First, the source areas sampled by the soil heat flux plates ($cm^2$ scale), net radiometer ($m^2$ scale), and EC vary between one another by up to several orders of magnitude. Therefore, variations in the surface conditions (e.g., slope geometry and sun facing angle, presence of rocks and standing/fallen deadwood) and climate within the different source areas likely induced systematic biases in the energy balance calculation. Second, while the poorer energy balance closure observed during neutral-and-stable-daytime relative to unstable-daytime periods could be due in part to heat storage in the air beneath the EC sensors, this effect was unlikely to be substantial because of the short height of the EC system and near-absence of a canopy in the EC system source areas. Third, advection associated with wind speed gradients could, in principal, bias EC heat fluxes similarly to $CO_2$. Since we observed (1) no systematic relationship between $\overline{w}$ and the relative difference between $H+\mathrm{LE}$ and $\mathrm{Rn}-G$ and (2) substantially greater bias in EC heat flux versus available energy measurements than in EC versus footprint $CO_2$ fluxes, it is likely that the role of advection is minor relative to other factors such as difference in source area in the lack of energy balance closure at the HLTK.

### 5.2. Influence of meteorological forcing on surface $CO_2$ fluxes

Lewicki et al. (2007) showed that large spatio-temporal variations in surface $CO_2$ fluxes measured by the chamber method at the HLTK from 09/12/2006 to 09/21/2006 were meteorologically driven. They calculated total $CO_2$ discharge rates for the study area based on chamber measurements and found them to be positively correlated with average daily atmospheric pressure and inversely correlated with average daily wind speed, most strongly at 1-day time lag. While the processes driving these relationships likely involved complex interactions between meteorology, topography, and vadose zone gas flow, Lewicki et al. (2007) suggested that spatio-temporal changes in surface $CO_2$ fluxes may have been primarily due to dynamic coupling between the flow of volcanic $CO_2$ at depth within the vadose zone and wind.

Despite the complications introduced into the EC $CO_2$ flux time series by the temporally varying flux source area, we observed similar relationships between average daily EC $CO_2$ fluxes and average daily wind speed and atmospheric pressure from 09/08/2006 to 09/22/2006 (zone I, Fig. 5a and b) to those observed by Lewicki et al. (2007) for chamber measurements over a similar time period. The relatively high degree of correlation observed between average daily EC $CO_2$ flux and wind speed from 09/08/2006 to 09/22/2006 was likely due to the cold front that passed through the region during that time bringing high winds that could have modulated vadose zone gas flow (Lewicki et al., 2007). However, from 09/24/2006 to 10/10/2006 (zone II, Fig. 5), EC $CO_2$ flux was more strongly correlated with atmospheric pressure and more weakly correlated with wind speed. This was probably due to the lower magnitude variations in average daily wind speed over this time period having less influence on subsurface gas flow to the atmosphere. Overall, our results indicate that similar to the chamber method, EC can be used to monitor background changes in volcanic $CO_2$ fluxes driven by meteorological forcing, and presumably changes related to deeply derived processes such as volcanic activity.

It is likely that precipitation events, and associated increases in soil moisture content also affected surface $CO_2$ fluxes at the HLTK. However, it was only possible to assess the relationship between EC $CO_2$ fluxes and precipitation in a limited fashion due to gaps in the time series of EC flux caused by data filtering for wind direction, $u_*$, and stationarity. This emphasizes the issue that potentially large gaps in time series of EC flux data must be tolerated, particularly at a site such as the HLTK. For example, we lost about half of the half-hour EC $CO_2$ flux data for the given wind direction range of interest (190 to 360°) due to insufficient turbulence and non-stationarity in the data. Automated and continuous chamber measurements at a fixed location within the study area (e.g., Rogie et al., 2001; Werner et al., 2003) would be valuable to supplement EC data.

## 6. Summary and conclusions

We measured a six-week time series of EC $CO_2$ and heat fluxes at the HLTK on Mammoth Mountain, a site with heterogeneous distribution of source fluxes and complex terrain that challenged the underlying assumptions of EC theory.

1. Half-hour EC $CO_2$ fluxes were compared with chamber fluxes measured repeatedly on a daily basis using footprint modeling. EC $CO_2$ fluxes were moderately correlated with, and on average unbiased relative to, footprint $CO_2$ fluxes. The average relative difference between HLTK EC and footprint $CO_2$ fluxes was similar to that reported for diffusely degassing areas at Solfatara volcano, Italy (Werner et al., 2003). Even though HLTK chamber $CO_2$ fluxes were measured on a daily basis, it was not possible to completely characterize spatio-temporal variations in source $CO_2$ fluxes on the timescale of the EC measurements. This factor, as well as advection of $CO_2$ due to topographic variations and the inherent random errors associated with both the EC and chamber methods likely contributed to the differences observed between $CO_2$ fluxes measured by the two techniques.
2. Average daily EC $CO_2$ fluxes were well correlated with average daily footprint $CO_2$ fluxes, indicating that when random error is reduced in $CO_2$ flux measurements by temporal averaging, the EC technique can perform well under certain complex site conditions. However, potential volcanic and geothermal sites for deployment of EC must be evaluated on an individual basis to assess viability of the method.
3. Turbulent heat fluxes were well correlated with available energy at the HLTK and the degree of energy balance closure fell within the range observed in many investigations

Author's personal copy



conducted in contrasting ecosystems and climates with more ideal terrain and surface flux characteristics.

4. Average daily EC $CO_2$ fluxes were correlated with both average daily wind speed and atmospheric pressure over the observation period, the degree to which depended on the magnitude of the fluctuations in the atmospheric parameters. The relationships between EC $CO_2$ fluxes and wind speed and atmospheric pressure were similar to those observed between chamber $CO_2$ fluxes and the atmospheric parameters over a comparable time period. Similar to the chamber method, EC can be used to monitor background changes in volcanic $CO_2$ fluxes driven by meteorological forcing, and presumably changes related to deeply derived processes such as volcanic activity.
5. EC provides the benefit over the chamber method of a time and space-averaged measurement of surface $CO_2$ flux that is essentially fully automated. However, potentially large gaps in time series of data must be tolerated with EC, depending on site characteristics and atmospheric conditions. Also, the spatial distribution of surface $CO_2$ fluxes cannot be mapped in detail by EC, as it can by the chamber method. The chamber and EC methods are therefore best used together, providing complementary information in volcanic gas surveillance programs.

## Acknowledgements

We thank C. Werner, an anonymous reviewer, and S. Biraud for comments that greatly improved the manuscript, T. Tosha and R. Aoyagi for assistance in the field, and H.P. Schmidt for the FSAM source code. This work was supported by the Zero Emissions Research and Technology (ZERT) program through the U.S. Department of Energy and the Ministry of Economy, Trade and Industry (METI) of Japan through the Lawrence Berkeley National Laboratory Sponsored Project Office Contract No. LB06002281.

## References

Anderson, D.E., Farrar, C.D., 2001. Eddy covariance measurement of $CO_2$ flux to the atmosphere from an area of high volcanogenic emissions, Mammoth Mountain, California. Chemical Geology 177, 31–42.

Aubinet, M., Grelle, A., Ibrom, A., et al., 2000. Estimates of the annual net carbon and water exchange of European forests: the EUROFLUX methodology. Advances in Ecological Research 30, 113–175.

Bailey, R.A., 1989. Geologic map of the Long Valley Caldera, Mono-Inyo Craters volcanic chain and vicinity, eastern California, scale 1:62,500. U.S. Geological Survey Miscellaneous Investigations Map, I—1933.

Baldocchi, D.D., 2003. Assessing the eddy covariance technique for evaluating carbon dioxide exchange rates of ecosystems: past, present, and future. Global Change Biology 9, 479–492.

Baldocchi, D.D., Hicks, B.B., Meyers, T.P., 1988. Measuring biosphere–atmosphere exchanges of biologically related gases with micrometeorological methods. Ecology 69, 1331–1340.

Baubron, J.-C., Allard, P., Sabroux, J.-C., Tedesco, D., Toutaln, J.P., 1991. Soil gas emanations as precursory indicators of volcanic eruptions. Journal of the Geological Society 148, 571–576.

Bergfeld, D., Goff, F., Janik, C.J., 2001. Elevated carbon dioxide flux at the Dixie Valley geothermal field, Nevada; relations between surface phenomena and the geothermal reservoir. Chemical Geology 177, 43–66.

Billesbach, D.P., Fischer, M.L., Torn, M.S., Berry, J.A., 2004. A portable eddy covariance system for the measurement of ecosystem–atmosphere exchange of $CO_2$, water vapor, and energy. Journal of Atmospheric and Oceanic Technology 21, 639–650.

Chiodini, G., Cioni, G.R., Guidi, M., Raco, B., Marini, L., 1998. Soil $CO_2$ flux measurements in volcanic and geothermal areas. Applied Geochemistry 13, 543–552.

Conen, F., Smith, K.A., 1998. A re-examination of closed flux chamber methods for the measurement of trace gas emissions from soils to the atmosphere. European Journal of Soil Science 49, 701–707.

Connor, C.B., Clement, B.M., Song, X.D., Lane, S.B., Westthomas, K., 1993. Continuous monitoring of high-temperature fumaroles on an active lava dome, Volcan Colima, Mexico — evidence of mass-flow variation in response to atmospheric forcing. Journal of Geophysical Research 98, 19,713–19,722.

Evans, W.C., Sorey, M.L., Kennedy, B.M., Stonestrom, D.A., Rogie, J.D., Shuster, D.L., 2001. High $CO_2$ emissions through porous media: transport mechanisms and implications for flux measurement and fractionation. Chemical Geology 177, 15–29.

Farrar, C.D., Sorey, M.L., Evans, W.C., Howle, J.F., Kerr, B.D., Kennedy, B.M., King, Y., Southon, J.R., 1995. Forest-killing diffuse $CO_2$ emission at Mammoth Mountain as a sign of magmatic unrest. Nature 376, 675–678.

Farrar, C.D., Neil, J.M., Howle, J.F., 1998. Magmatic carbon dioxide emissions at Mammoth Mountain, California. U.S. Geological Survey Water Resources Investigation Report 98–4217, 34 pp.

Folken, Th., Wichura, B., 1996. Tools for quality assessment of surface-based flux measurements. Agricultural and Forest Meteorology 78, 83–105.

Garratt, J.R., 1992. The Atmospheric Boundary Layer. Cambridge University Press, Cambridge, p. 316.

Gerlach, T.M., Doukas, M.P., McGee, K.A., Kessler, R., 1998. Three-year decline of magmatic $CO_2$ emissions from soils of a Mammoth Mountain tree kill: Horseshoe Lake, CA, 1995–1997. Geophysical Research Letters 25, 1947–1950.

Gerlach, T.M., Doukas, M.P., McGee, K.A., Kessler, R., 2001. Soil efflux and total emission rates of magmatic $CO_2$ at the Horseshoe Lake tree kill, Mammoth Mountain, California, 1995–1999. Chemical Geology 177, 101–116.

Granieri, D., Chiodini, G., Marzocchi, W., Avino, R., 2003. Continuous monitoring of $CO_2$ soil diffuse degassing at Phlegrean Fields (Italy): influence of environmental and volcanic parameters. Earth and Planetary Science Letters 212, 167–179.

Hernandez, P.A., Perez, N., Salazar, J.M., Nakai, S., Notsu, K., Wakita, H., 1998. Diffuse emissions of carbon dioxide, methane, and helium-3 from Teide volcano, Tenerife, Canary Islands. Geophysical Research Letters 25, 3311–3314.

Hernandez, P.A., Notsu, K., Salazar, J.M., Mori, T., Natale, G., Okada, H., Virgilli, G., Shimoike, Y., Sato, M., Perez, N.M., 2001. Carbon dioxide degassing by advective flow from Usu volcano, Japan. Science 2001, 83–86.

Hill, D.P., 1996. Earthquakes and carbon dioxide beneath Mammoth Mountain, California. Seismological Research Letters 67, 8–15.

Hill, D.P., Prejean, S.G., 2005. Volcanic unrest beneath Mammoth Mountain, California. Journal of Volcanology and Geothermal Research 146, 257–283.

Horst, T.W., Weil, J.C., 1992. Footprint estimation for scalar flux measurements in the atmospheric surface-layer. Boundary-Layer Meteorology 59, 279–296.

Kaimal, J.C., Finnigan, J.J., 1994. Atmospheric Boundary Layer Flows: Their Structure and Measurement. Oxford, Oxford University Press.

Klusman, R.W., Moore, J.N., LeRoy, M.P., 2000. Potential for surface gas measurements in exploration and surface evaluation of geothermal resources. Geothermics 29, 637–670.

Lee, X., 1998. On micrometeorological observations of surface-air exchange above tall vegetation. Agricultural and Forest Meteorology 91, 39–49.

Lewicki, J.L., Bergfeld, D., Cardellini, C., Chiodini, G., Granieri, D., Varley, Werner, C., 2005. Comparative soil $CO_2$ flux measurements and geostatistical estimation methods on Masaya volcano. Nicaragua, Bulletin of Volcanology 68, 76–90. doi:10.1007/s00445-005-0423-9.

Lewicki, J.L., Hilley, G.E., Tosha, T., Aoyagi, R., Yamamoto, K., Benson, S.M., 2007. Dynamic coupling of volcanic $CO_2$ flow and wind at the Horseshoe Lake tree kill, Mammoth Mountain, California. Geophysical Research Letters 34, L03401. doi:10.1029/2006GL028848.

Author's personal copy



McGee, K.A., Gerlach, T.M., 1998. Annual cycle of magmatic $CO_2$ in a tree-kill soil at Mammoth Mountain, California: implications for soil acidification. Geology 26, 463–466.

McGee, K.A., Gerlach, T.M., Kessler, R., Doukas, M.P., 2000. Geochemical evidence for a magmatic $CO_2$ degassing event at Mammoth Mountain, California, September–December 1997. Journal of Geophysical Research 105, 8447–8456.

Rahn, T.A., Fessenden, J.E., Wahlen, M., 1996. Flux chamber measurements of anomalous $CO_2$ emission from the flanks of Mammoth Mountain, California. Geophysical Research Letters 23, 1861–1864.

Rogie, J.D., Kerrick, D.M., Sorey, M.L., Chiodini, G., Galloway, D.L., 2001. Dynamics of carbon dioxide emission at Mammoth Mountain, California. Earth and Planetary Science Letters 188, 535–541.

Schmid, H.P., 1997. Experimental design for flux measurements: matching scales of observations and fluxes. Agricultural and Forest Meteorology 87, 179–200.

Turnipseed, A.A., Anderson, D.E., Blanken, P.D., Baugh, W.M., Monson, R.K., 2003. Airflows and turbulent flux measurements in mountainous terrain part 1. Canopy and local effects. Agricultural and Forest Meteorology 119, 1–21.

Turnipseed, A.A., Anderson, D.E., Burns, S., Blanken, P.D., Monson, R.K., 2004. Airflows and turbulent flux measurements in mountainous terrain part 2. Mesoscale effects. Agricultural and Forest Meteorology 125, 187–205.

Webb, E.K., Pearman, G.I., Leuning, R., 1980. Correction of flux measurements for density effects due to heat and water vapour transfer. Quarterly Journal of Royal Meteorological Society 106, 85–100.

Welles, J.M., Demetriades-Shah, T.H., McDermitt, D.K., 2000. Considerations for measuring ground $CO_2$ effluxes with chambers. Chemical Geology 177, 3–13.

Werner, C., Cardellini, C., 2006. Comparison of carbon dioxide emissions with fluid upflow, chemistry, and geologic structures at the Rotorua geothermal system, New Zealand. Geothermics 35, 221–238.

Werner, C., Wyngaard, J.C., Brantley, S.L., 2000. Eddy-correlation measurement of hydrothermal gases. Geophysical Research Letters 27, 2925–2928.

Werner, C., Chiodini, G., Voigt, D., Caliro, S., Avino, R., Russo, M., Brombach, T., Wyngaard, J., Brantley, S., 2003. Monitoring volcanic hazard using eddy covariance at Solfatara volcano, Naples, Italy. Earth and Planetary Science Letters 210, 561–577.

Werner, C., Chiodini, G., Granieri, D., Caliro, S., Avino, R., Russo, M., 2006. Eddy covariance measurements of hydrothermal heat flux at Solfatara volcano, Italy. Earth and Planetary Science Letters 244, 72–82.

Wilczak, J.M., Oncley, S.P., Stage, S.A., 2001. Sonic anemometer tilt correction algorithms. Boundary Layer Meteorology 99, 127–150.

Wilson, K., Goldstein, A., Falge, E., Aubinet, M., Baldocchi, D., Berbigier, P., Bernhofer, C., Ceulemans, R., Dolman, H., Field, C., Grelle, A., Ibrom, A., Law, B.E., Kowalski, A., Meyers, T., Moncrieff, J., Monson, R., Oechel, W., Tenhunen, J., Valentini, R., Verma, S., 2002. Energy balance closure at FLUXNET sites. Agricultural and Forest Meteorology 113, 223–243.